Supporting Materials

Enhanced rare earth element recovery from NdFeB leachates using magnetically responsive vermiculite–alginate nanocomposites

Giani de Vargas Brião [1], Claudia Batista Lopes (✉)[2], Ana Cristina Estrada [2], Tito Trindade [2], Carlos Manuel Silva [2,3], Meuris Gurgel Carlos da Silva [1], Melissa Gurgel Adeodato Vieira (✉)[1]

1 School of Chemical Engineering, University of Campinas, Campinas 13083-852, Brazil
2 Department of Chemistry, CICECO- Aveiro Institute of Materials, University of Aveiro, Aveiro 3810-193, Portugal
3 CERES- Department of Chemical Engineering, University of Coimbra, Faculty of Sciences and Technology, Coimbra 3030-790, Portugal

✉ Corresponding authors
E-mail: claudia.b.lopes@ua.pt (C. Lopes); melissag@unicamp.br (M. Vieira)

1. Chemicals and Materials

Iron(II) sulfate pentahydrate (99 %, Panreac Quimica S.A., Spain), calcium chloride dihydrate (EMSURE, P.A., Germany), alginic acid sodium salt powder (Sigma Aldrich), potassium hydroxide (P.A., LabChem, USA), potassium nitrate (97.7%, LabChem, USA), and expanded vermiculite (Brazil Minérios S.A., Brazil) were used in the synthesis of the magnetic materials.

The metal solutions were prepared by dissolving their salts in ultrapure water. Salts of Fe(II), Zn(II), Pr(III), Co(II), Nd(III), Dy(III), Mn(II), Ni(II), and Al(III) were used. Details are listed in Table S1.

The eluent solutions were prepared using salts – ammonium chloride (NH_4Cl), and magnesium(II) dichloride hexahydrate ($MgCl_2 \cdot 6H_2O$) –, complexing agents – diethylenetriaminepentaacetic acid (DTPA), disodium ethylenediaminetetraacetate dihydrate ($Na_2EDTA \cdot 2H_2O$) –, and strong acids – nitric acid (HNO_3) and hydrochloric acid (HCl). The purities and suppliers of the eluents are compiled in Table S2.

Table S1 REM salts used to prepare the multimetal solution.

Salt	Supplier
Iron(II) sulfate pentahydrate	99 %, Panreac Quimica S.A. (Spain)
Zinc(II) nitrate hexahydrate	99 %, Sigma-Aldrich (Germany)
Praseodymium(III) nitrate hexahydrate	99 %, Sigma Aldrich (Germany)
Cobalt(II) chloride hexahydrate	98 %, Panreac Quimica S.A. (Spain)
Neodymium(III) nitrate hexahydrate	99.9 %, Sigma Aldrich (Germany)
Dysprosium(III) nitrate hexahydrate	99.9 %, Sigma-Aldrich (Germany)
Manganese(II) sulfate monohydrate	99 %, Panreac Quimica (Spain)
Nickel(II) chloride hexahydrate	99.99 %, Merck (Germany)
Aluminum(III) sulfate octadecahydrate	P.A., Pancreac Quimica (Spain)

Table S2 Eluents used in the desorption experiments.

Eluent	Supplier
Ammonium chloride	99.8 %, Pronalab (Portugal)
Magnesium(II) dichloride hexahydrate	P.A., Fagron (Belgium)
Diethylenetriaminepentaacetic acid	97%, Aldrich (Germany)
Disodium ethylenediaminetetraacetate dihydrate	97 %, Fluka (Germany)
Nitric acid	65 %, Applied Chemicals (Switzerland)
Hydrochloric acid	37 %, VWR (USA)

2. Modelling methods

2.1 Kinetic modeling

Kinetic constants were obtained by nonlinear fitting of the models to the experimental data, such pseudo-first order (PFO, Equation S1) (Lagergren, 1898), pseudo-second order (PSO, Equation S2) (Ho and McKay, 1998a), Elovich (Equation S3)(Aharoni and Tompkins, 1970; Wu et al. 2009), Weber and Morris (Equation S4) (Weber and Morris, 1963) and Boyd (Equation S5-S9) (Boyd et al., 1947; Viegas et al., 2014) models.

$$q_t = q_e(1 - e^{-k_1 t}) \qquad \text{(S1)}$$

$$q_t = \frac{k_2\ q_e^2\ t}{1 + k_2\ q_e\ t} \qquad \text{(S2)}$$

where k_1 (1/min) and k_2 (g/(μmol min)) are the PFO and PSO rate constants, q_t and q_e are the solid loadings at a specific time and at the equilibrium (μmol/g), and t is the time (min).

Elovich model is represented by:

$$q_t = \left(\frac{1}{\beta}\right)\ln(1 + \alpha\beta t) \qquad \text{(S3)}$$

where α is the initial sorption rate (μmol/(g min)), and β is the Elovich constant (g/μmol).

The Weber and Morris model describes sorption kinetics assuming intraparticle diffusion:

$$q_t = k_i\sqrt{t} + I \qquad \text{(S4)}$$

where k_i is the rate constant of intraparticle diffusion (μmol/(g.√min)) and *I* is the term that refers to the boundary layer (intercept). The higher the *I* value, the higher the boundary layer effect on the mass transfer.

The Boyd diffusion model can predict which step limits the mass transfer process of adsorption. According to this method, the solute fraction sorbed up until *t (F(t))* can be calculated by:

$$F(t) = \frac{q_t}{q_e} \quad \text{(S5)}$$

$$F(t) = 1 - \frac{6}{\pi^2}\sum_{n=1}^{\alpha}\frac{1}{n^2}e(-n^2 B_t) \quad \text{(S6)}$$

B_t can be calculated by equations S7 and S8 through a simplification of Equation S6 by Fourier transform and numeric integration.

$$0 \leq F \leq 0.85: B_t = 2\pi - \frac{\pi^2 F}{3} - 2\pi\left(1 - \frac{\pi F}{3}\right)^{1/2} \quad \text{(S7)}$$

$$0.85 < F \leq 1: B_t = -0.4977 - ln(1 - F) \quad \text{(S8)}$$

The plot of B_t *versus t* specifies the rate-limiting step. If a linear equation fits the data, with null y-intercept, intraparticle diffusion governs the process, otherwise, film diffusion is the rate-limiting step. The angular coefficient (*B*) of the linear fit of B_t *versus t*, is related to the effective diffusivity according to:

$$B = \frac{D_{ef}\pi^2}{r^2} \quad \text{(S9)}$$

where D_{ef} is the effective coefficient of diffusion of the metal on the adsorbent (m²/min) and r is the average size of particles adsorbent (m).

2.2 Equilibrium modeling

Equilibrium isotherms with two and three parameters were fitted to data. The two-parameter isotherms are the Freundlich (Freundlich, 1906) (Equation S10), Langmuir (Langmuir, 1918) (Equation S11), and Dubinin-Radushkevich (Equations S12 – S14) (Dubinin and Radushkevich 1947) models.

$$q_e = K_F C_e^{n_F} \quad \text{(S10)}$$

$$q_e = \frac{q_{mL} K_L C_e}{1 + (K_L C_e)} \quad \text{(S11)}$$

$$q_e = q_{mD} e^{-B_D \varepsilon^2} \quad \text{(S12)}$$

$$\varepsilon = \mathrm{RTln}\left(1 + \frac{1}{C_e / 10^6}\right) \quad \text{(S13)}$$

$$\mathrm{E} = \frac{1}{\sqrt{2B_D}} \quad \text{(S14)}$$

where K_L (L/μmol) and q_{mL} (μmol/g) are the Langmuir constant and sorption capacity, respectively; K_F (μmol/(g (μmol/L)$^{-1/nF}$)) and n_F are the Freundlich constant and heterogeneity factor, respectively; B_D is the constant associated with the free energy of adsorption (mol²/J^2), ε is the Polanyi potential (J/mol), R is the ideal gas constant (8.314 J/(mol K)), T is the temperature (K), E is the free energy of adsorption (J/mol).

The three-parameter models are Brunauer-Emmett-Teller (BET, Equation S15) (Brunauer et al. 1938), Sips (Equation S16) (Sips, 1948) and Toth (Equation S17) (Tóth, 1995, 1997).

$$q_e = \frac{q_{mB} K_B C_e}{(1 - K_u C_e)(1 - K_u C_e + K_B C_e)} \quad \text{(S15)}$$

$$q_e = \frac{q_{mS} K_S {C_e}^{m_S}}{1 + (K_S C_e)^{m_S}} \quad \text{(S16)}$$

$$q_e = \frac{q_{mT} C_e}{(K_T + C_e^{t_n})^{1/t_n}} \quad \text{(S17)}$$

where q_{mB} is the sorption capacity of the first layer (μmol/g), K_B is the equilibrium constant of sorption for the first layer (L/μmol), and K_u is the equilibrium constant of adsorption for upper layers (L/μmol); q_{mS} and K_S are the Sips maximum capacity (μmol/g) and constant (L/μmol), and m_S is the dimensionless heterogeneity factor; q_{mT} is defined as the maximum adsorption capacity (μmol/g), K_T is the constant of the Toth equation; and t_n is a dimensionless parameter known as Toth constant and represents the inhomogeneity of the solid surface and is usually lower than 1. If the value of t_n equals 1, the Toth model reduces to the Langmuir model, indicating homogeneous sorption.

2.3 Assessment of data correlation quality

The statistical parameters to evaluate the goodness of fit of the kinetic models were the adjusted coefficient of determination (R^2_{adj}) (Equation S18), the sum of squared errors ($S_{y.x}$) (Equation S19), and the Akaike information criterion (AIC)(Equation S20).

$$R^2_{adj} = 1 - \left[\frac{(1 - \frac{\sum_{i=1}^{N}(y_i - \hat{y}_i)^2}{\sum_{i=1}^{N}(y_i - \bar{y})^2})(N-1)}{N - K - 1} \right] \quad \text{(S18)}$$

$$S_{y,x} = \sqrt{\frac{\sum(residual^2)}{N - K}} \quad \text{(S19)}$$

$$AIC = N \ln\left(\frac{Sum\ square\ of\ errors}{N}\right) + 2K \quad \text{(S20)}$$

where *N* is the number of points, y_i and $\hat{y}_i$ are the experimental and predicted values, respectively, $\bar{y}$ is the mean of the experimental values, and *K* is the number of estimable parameters plus one (for the variance) (Hurvich and Tsai, 1989).

3. Supplementary Figures

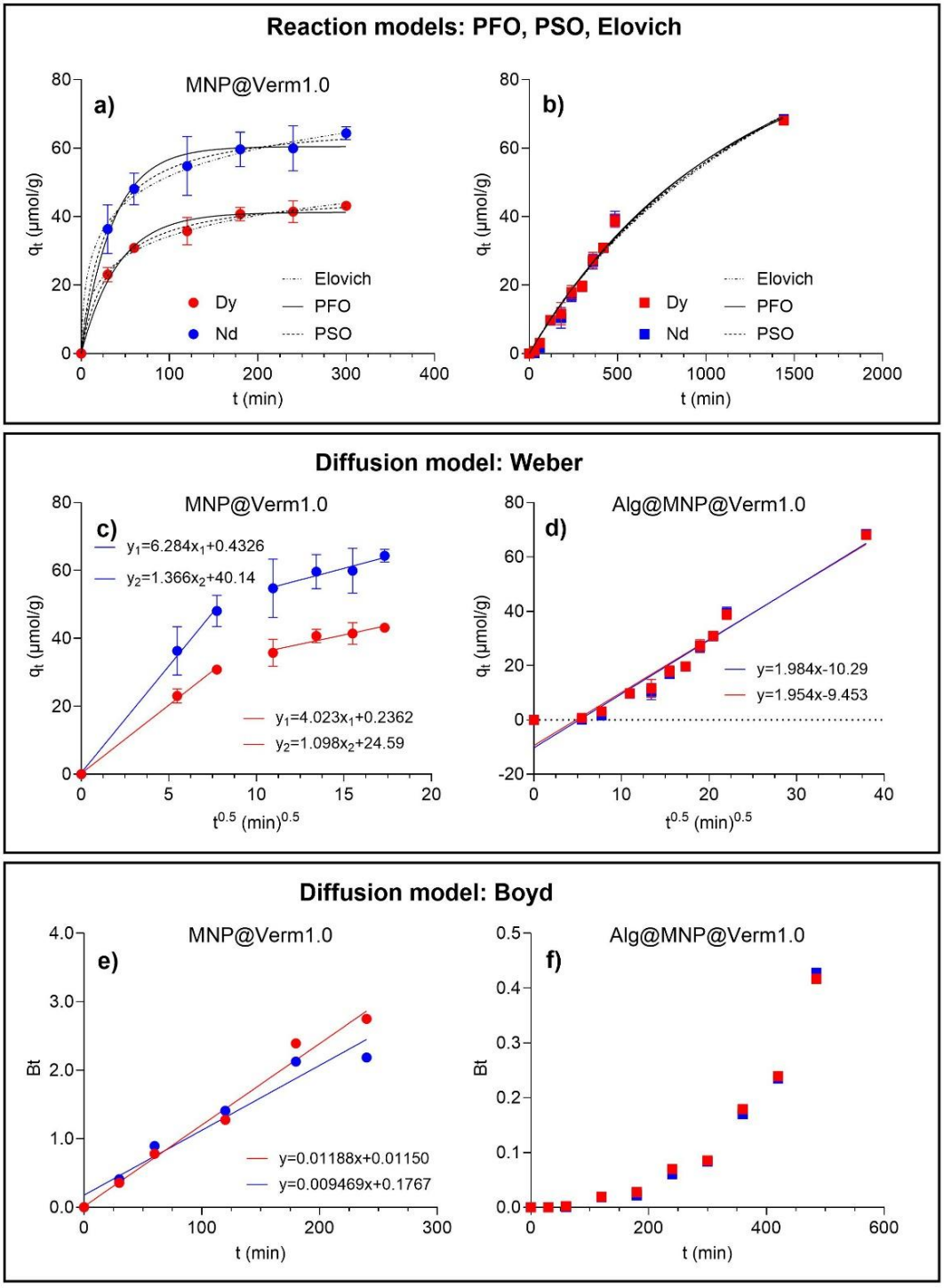

Fig. S1 Sorption of Nd(III) and Dy(III) over time on MNP@Verm1.0 (a, c, and e) and Alg@MNP@Verm1.0 (b, d, f) nanocomposites, with the corresponding fits of the kinetic models: PFO and PSO (a and b); Weber and Morris (c and d), and Boyd (e and f)).

4. Supplementary Tables

Table S3 Elemental composition (%) of MNP@Verm.10 and Alg@MNP@Verm1.0 determined by SEM-EDS analysis.

Element	Samples	
	MNP@Verm1.0	Alg@MNP@Verm1.0
C	-	18.85
O	47.28	47.8
Mg	6.64	2.97
Al	3.11	1.4
Si	8.18	4.03
Cl	-	0.86
K	1.55	0.17
Ca	-	4.32
Ti	0.23	0.14
Fe	33.01	19.46

Table S4 Best-fit parameters of the reaction and diffusion models.

Model	Parameters	MNP@Verm1.0		Alg@MNP@Verm1.0	
		Nd(III)	Dy(III)	Nd(III)	Dy(III)
Reaction models					
PFO	k_1 (1/min)	2.79x10^{-2}	2.39x10^{-2}	8.96x10^{-4}	9.51x10^{-4}
	q_e (µmol/g)	60.4	41.2	95.6	92.2
	R^2_{adj}	0.987	0.985	0.980	0.986
	AIC	24.9	20.6	30.7	26.0
	$S_{y,x}$	2.58	1.89	2.91	2.35
PSO	k_2 (g/µmol min)	5.60x10^{-4}	6.51 x10^{-4}	3.65x10^{-6}	4.16x10^{-6}
	q_e (µmol/g)	68.1	47.3	154.9	147.2
	R^2_{adj}	0.997	0.998	0.978	0.985
	AIC	13.7	7.98	31.6	27.2
	$S_{y,x}$	1.16	0.770	3.03	2.48
Elovich	α (µmol/g min)	10.1	4.13	8.99x10^{-2}	1.74x10^{-2}
	β (g/µmol)	8.64 x10^{-2}	1.13 x10^{-2}	1.62 x10^{-2}	9.30 x10^{-2}
	R^2_{adj}	0.995	0.996	0.976	0.983
	AIC	18.6	10.8	32.5	28.4
	$S_{y,x}$	1.64	0.938	3.15	2.61
Diffusion models					
Weber and Moris	*1st linear segment*				
	k_i (µmol/g min$^{0.5}$)	6.28	4.02	1.98	1.95
	$intercept$	0.433	0.236	-10.3	-9.45
	$95\%\ C.I.$	-22.6 to 10.5	-12.3 to 12.8	-16.9 to -3.66	-15.5 to -3.42
	R^2	0.997	0.998	0.944	0.952
	$S_{y,x}$	1.86	1.02	5.13	4.67
	2nd linear segment				
	k_i (µmol/g min$^{0.5}$)	1.37	1.10	n.a.	n.a.
	$intercept$	40.1	24.6	n.a.	n.a.
	$95\%\ C.I.$	22.3 to 58.0	8.57 to 40.6	n.a.	n.a.
	R^2	0.919	0.902	n.a.	n.a.
	$S_{y,x}$	1.36	1.22	n.a.	n.a.
Boyd	$slope$	0.00947	0.0119	n.a.	n.a.
	$intercept$	0.177	0.0115	n.a.	n.a.
	D_{ef} (m^2/min)	1.08 x 10^{-15}	1.36 x10^{-15}		
	$95\%\ C.I.$	-0.223 to 0.576	-0.276 to 0.300	n.a.	n.a.
	R^2	0.951	0.984	n.a.	n.a.
	$S_{y,x}$	0.221	0.159	n.a.	n.a.

Table S5 Equilibrium isotherm models fitted to the sorption of Nd(III) and Dy(III) on MNP@Verm1.0 and Alg@MNP@Verm1.0 nanocomposites.

Model	Parameters	MNP@Verm1.0		Alg@MNP@Verm1.0	
		Nd(III)	Dy(III)	Nd(III)	Dy(III)
Two-parameter isotherms					
Freundlich	K_F (μmol/g·(μmol/L)$^{-1/nF}$)	49.2	29.4	44.0	42.6
	n_F(-)	3.35	4.50	2.99	2.89
	R^2_{adj}	0.891	0.835	**0.961**	**0.965**
	$S_{y,x}$	9.75	6.39	**5.84**	**5.52**
	AIC	46.1	37.6	**40.3**	**39.3**
Langmuir	q_{mL} (μmol/g)	84.9	44.3	91.8	92.3
	K_L (L/μmol)	2.39	5.73	0.977	0.897
	R^2_{adj}	**0.991**	**0.959**	0.917	0.920
	$S_{y,x}$	**2.85**	**3.20**	8.51	8.30
	AIC	**26.4**	**27.9**	47.1	46.6
Dubinin-Radushkevich	q_{mD} (μmol/g)	76.3	42.5	80.8	80.9
	B_D (mol²/J²)	5.80×10^{-8}	2.74×10^{-8}	2.67×10^{-7}	3.05×10^{-7}
	R^2_{adj}	0.961	0.950	0.856	0.852
	$S_{y,x}$	5.82	3.51	11.2	11.3
	AIC	37.9	29.2	52.1	52.2
Three-parameter isotherms					
BET	K_B (L/μmol)	2617	(1)	134	114
	q_{mB} (μmol/g)	84.4	44.3	58.7	58.4
	C_S (L/μmol)	1081	1.20×10^{15}	23.9	24.0
	R^2_{adj}	0.989	0.948	0.936	0.942
	$S_{y,x}$	3.12	3.58	7.51	7.09
	AIC	35.8	41.9	50.6	49.6
Sips	K_S (L/μmol)	2.23	4.83	0.360	0.313
	q_{mS} (μmol/g)	86.1	44.8	174	186
	n_S (-)	0.957	0.926	0.474	0.477
	R^2_{adj}	0.989	0.949	0.963	0.966
	$S_{y,x}$	3.08	3.54	5.71	5.46
	AIC	35.6	41.8	45.7	44.9
Toth	q_{mT} (μmol/g)	84.7	53.7	47.6	46.1
	K_T (L/ μmol)	0.416	0.295	0.0313	0.0353
	t_n (-)	1.00	0.908	1.40	1.43
	R^2_{adj}	0.989	0.957	0.960	0.964
	$S_{y,x}$	3.12	3.25	5.89	5.60
	AIC	35.8	40.6	46.3	45.4

(1) identified as unstable parameter by the analysis software

Table S6 Summary of the XPS binding energies, FWHM (eV), and atomic percentages for the chemical elements detected in MNP@Verm1.0 and Alg@MNP@Verm1.0 before and after the sorption of Nd(III) and Dy(III) (loaded-MNP@Verm1.0 and loaded-Alg@MNP@Verm1.0).

Spectral line	MNP@Verm1.0			Loaded-MNP@Verm1.0		
Name	Peak BE (eV)	FWHM (eV)	Atomic (%)	Peak BE (eV)	FWHM (eV)	Atomic (%)
Al 2p	74.51	2.42	5.6	-	-	-
Al 2s	-	-	-	120.8	4.9	6.59
Si 2s	153.87	3.19	11.78	-	-	-
C 1s	285.18	2.86	6.54	286.34	4.18	5.59
K 2p3	293.92	1.92	0.86	-		
O 1s	531.65	3.46	58.45	532.6	4.65	61.6
F 1s	685.65	2.18	0.44	686.96	3.53	0.49
Fe 2p	711.2	4.69	7.54	711.55	4.34	6.27
Mg 1s	1304.24	2.6	8.79	1305.21	3.34	7.88
Si 2p	-	-	-	104.13	3.65	11.58
Spectral line	Alg@MNP@Verm1.0			Loaded-Alg@MNP@Verm1.0		
Name	Peak BE (eV)	FWHM (eV)	Atomic (%)	Peak BE (eV)	FWHM (eV)	Atomic (%)
Al 2p	73.72	1.73	0.96	-	-	-
Al 2s	-	-	-	119.27	4.89	5.56
Mg 2s	88.46	2.35	1.21	-	-	-
Si 2p	102.1	2.47	3.05	102.35	2.85	6.01
P 2p	-	-	-	133.66	2.66	1.82
Cl 2p	198.29	3.07	3.46	-	-	-
C 1s	285.65	4.52	45.3	285.44	3.57	36.51
Ca 2p3	347.23	2.21	4.7	347.47	2.23	2.08
O 1s	531.98	3.29	39.91	532.12	3.39	43.18
Fe 2p	710.74	6.03	1.16	724.03	4.51	1.3
Cu 2p	-	-	-	953.02	2.88	0.48
Na1s	1071.8	1.38	0.25	-	-	-
Mg 1s	-	-	-	1304.22	2.98	3.07

Table S7 Simulated NdFeB magnet leachate solution, pH = 3.5.

Components	Al	Co	Dy	Fe	Mn	Nd	Ni	Pr	Zn
C_0 (mmol/L)	0.034	0.12	0.048	7.27	0.015	0.74	0.026	0.26	0.43

References of Supporting Information

Aharoni C, Tompkins FC (1970) Kinetics of Adsorption and Desorption and the Elovich Equation. In: Eley DD; PH; WPB (ed) Advances in Catalysis. Academic Press, pp 1–49

Boyd GE, Adamson AW, Myers LS (1947) The Exchange Adsorption of Ions from Aqueous Solutions by Organic Zeolites. II. Kinetics. J Am Chem Soc 69:2836–2848. https://doi.org/10.1021/ja01203a066

Brunauer S, Emmett PH, Teller E (1938) Adsorption of Gases in Multimolecular Layers. J Am Chem Soc 60:309–319. https://doi.org/10.1021/ja01269a023

Dubinin MM, Radushkevich LV (1947) The equation of the characteristic curve of activated charcoal. Proceedings of the Academy of Sciences of USSR 55:331

Freundlich HMF (1906) Over the Adsorption in Solution. Journal of Physical Chemistry 57:385–470

Ho YS, McKay G (1998) A Comparison of chemisorption kinetic models applied to pollutant removal on various sorbents. Process Safety and Environmental Protection 76:332–340. https://doi.org/10.1205/095758298529696

Hurvich CM, Tsai CL (1989) Regression and time series model selection in small samples. Biometrika 76:297–307. https://doi.org/10.1093/biomet/76.2.297

Lagergren S (1898) About the theory of so-called adsorption of soluble substances. Kungliga Suensk Vetenskapsak ademiens Handlingar 24:1–39

Langmuir I (1918) The Adsorption of Gases on Plane Surfaces of Glass Mic and Platinum. Journal of American Chemical Society 40:1361–1403

Sips R (1948) On the structure of a catalyst surface. J Chem Phys 16:490–495. https://doi.org/10.1063/1.1746922

Tóth J (1995) Uniform interpretation of gas/solid adsorption. Adv Colloid Interface Sci 55:1–239. https://doi.org/10.1016/0001-8686(94)00226-3

Tóth J (1997) Some Consequences of the Application of Incorrect Gas/Solid Adsorption Isotherm Equations. J Colloid Interface Sci 185:228–235. https://doi.org/10.1006/jcis.1996.4562

Viegas RMC, Campinas M, Costa H, Rosa MJ (2014) How do the HSDM and Boyd's model compare for estimating intraparticle diffusion coefficients in adsorption processes. Adsorption 20:737–746. https://doi.org/10.1007/s10450-014-9617-9

Weber WJ, Morris JC (1963) Kinetics of adsorption carbon from solutions. Journal Sanitary Engineering Division Proceedings 89:31–60

Wu F-C, Tseng R-L, Juang R-S (2009) Characteristics of Elovich equation used for the analysis of adsorption kinetics in dye-chitosan systems. Chemical Engineering Journal 150:366–373. https://doi.org/10.1016/j.cej.2009.01.014